Journal of Ceramic Processing Research. Vol. 17, No. 10, pp. 1100~1105 (2016)

J O U R N A L O F
Ceramic Processing Research

Effect of the content of light-burned alumina-spinel composite on the slag resistance of corundum-spinel refractory castables

Qingjie Chen, Wen Yan*, Nan Li, Xiaoli Lin, Bingqiang Han and Yaowu Wei
The State Key Laboratory of Refractories and Metallurgy, Wuhan University of Science and Technology, Wuhan, China

Corundum-spinel castable is widely used in ladles. The type of spinel impacts the slag resistance of castables. Spinel formed in situ enhances penetration resistance but pre-synthesized spinel enhances corrosion resistance of castable. A light-burned alumina-spinel composite (LBC) was used as spinel source in this study for a balance between the penetration and corrosion resistance. The effects of the LBC content on the penetration and corrosion resistance of the castables were studied by means of crucible test. The phase compositions and lattice distortions of the spinels in alumina-spinel composites were studied by X-ray diffractometry (XRD) and the microstructures of the samples eroded were studied by scanning electron microscopy (SEM). The results indicated that the penetration resistance increased and corrosion resistance of slag decreased with increasing in LBC content because of its smaller crystallite size and higher lattice distortion, as well as smaller particle size. The optimized LBC content is 17.6 wt%.

Key words: Corundum-spinel castables, Light-burned alumina-spinel composite, Penetration resistance, Corrosion resistance.

Introduction

Corundum-spinel refractory castables have been widely used as working lining of steel ladle because of their excellent slag resistance [1-5]. There have been some studies on the effects of in-situ and pre-synthesized spinels on the slag resistance of corundum-spinel castables [6-9]. Fuhrer et al. [10] found that the sample with in-situ spinel had higher corrosion resistance than that with pre-synthesized spinel, because in-situ spinel could absorb more Mn and Fe ions from the slag. Fang el al. [11] studied the effect of spinel on the slag resistance of the unfired corundum-spinel brick and found that the slag resistance of the brick was enhanced by the pre-synthesized spinel because of its great grain size. These results seem contrary. Some results suggested using the in-situ spinel with small grain size and the other results suggested using the pre-synthesized spinel with bigger grain size. In our previous work [12], we found that the lattice strain of spinel affected the slag resistance. It is clear that pre-synthesized spinel has lower dissolution rate into slag and higher corrosion resistance because it has more complete crystal structure and larger grain size; however, the in-situ spinel has higher penetration resistance because of its higher lattice strain of crystal which can trap more Mn and Fe ions, resulting in that the slag becomes more viscous.

It is an interesting question whether a type of spinel can get an optimized balance between corrosion and penetration resistance of castables. The light-burned alumina-spinel composite (LBC) synthesized at lower temperature may be appropriate. A LBC with 90 wt% of Al_2O_3 was chosen for investigation in this work. The effect of LBC content on penetration and corrosion resistances of the corundum-spinel castables has been studied.

*Corresponding author:
Tel : +86-027-68862511
Fax: +86-027-68862121
E-mail: yanwen@wust.edu.cn

Experimental Procedure

Raw materials

The raw materials used in this investigation were tabular alumina (≤ 5 mm, Zili Refractory Technologies Co. Ltd., China), dead-burned alumina-spinel composite powder (DBC, Jinghui Refractory Technologies Co. Ltd., China), micro alumina (≤ 5 μm, Special Refractories Technologies Co. Ltd., China), microsilica (971U, Elkem, Kristiansand, Norway) and calcium alumina cement (CAC, CA80, GaoDa New Type Refractory Material Factory, China). LBC powder was prepared in our lab and fired at 1600 °C for 3 h. The Chemical compositions of the raw materials are listed in Table 1. The XRD patterns of LBC and DBC are shown in Fig. 1.

The lattice strains, lattice parameters and crystallite sizes of spinels in LBC and DBC and the phase compositions and particle sizes of LBC and DBC powders are given in Table 2. It is found that the spinel in LBC has higher lattice strain but smaller crystallite and particle sizes than DBC. Also, the spinel in LBC has smaller lattice parameter than that in DBS. It indicates that the alumina content of spinel in LBC is higher than that in DBC because increasing alumina content in spinel will decrease the lattice parameter of

Table 1. Chemical compositions of the raw materials (wt%).

s	DBC	LBC	Tabular alumina	Micro alumina	Microsilica	CAC
MgO	10.81	9.43	–	–	0.11	0.04
Al_2O_3	88.29	89.91	99.42	97.69	0.59	76.07
CaO	0.30	0.27	–	–	0.42	19.96
SiO_2	0.30	0.22	0.02	0.15	96.58	0.51
Fe_2O_3	0.29	0.10	0.02	0.19	0.16	0.32
K_2O	–	0.06	–	–	–	0.25
Na_2O	–	–	0.36	0.35	–	0.10

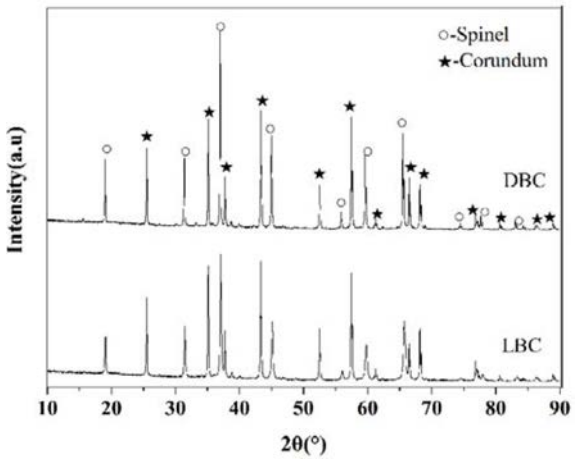

Fig. 1. XRD patterns of LBC and DBC powders.

spinel [13]. The differences of phase compositions between LBC and DBC are a little.

Preparation of specimens

Four corundum-spinel refractory castables were selected for the corrosion tests and they were prepared according to the formulas listed in Table 3. They have the same chemical composition and the same alumina-spinel composite content of 23.5 wt%. The four castables were named as L0, L11.8, L17.6 and L23.5 according to their LBC contents (0 wt%, 11.8 wt%, 17.6 wt% and 23.5 wt%).

The rectangular parallelepiped specimens (150 mm length × 25 mm width × 25 mm thickness) were casted for apparent porosity and bulk density measurement. For the corrosion tests, the cubic crucibles (70 mm × 70 mm × 70 mm) with an internal hole of 30 mm diameter and 40 mm depth were prepared. They were cured for 24 hrs at room temperature and then dried at 110 ºC for 24 hrs. The rectangular parallelepiped specimens and the crucibles filled with 30 g of slag were heated at 1600 ºC for 3 hrs in an electric chamber furnace and then cooled to room temperature. The composition of slag is given in Table 4.

After the experiments, the corroded samples were cross-sectioned perpendicular to the slag-refractory interface, as shown in Fig. 2. In addition, the corrosion

Table 3. Compositions of batching mixtures of the castables (wt%).

Raw Materials	L0	L11.8	L17.6	L23.5
Tabular alumina (d ≤ 5 μm)	70	70	70	70
LBC powder (d ≤ 45 μm)	0	11.8	17.6	23.5
DBC powder (d ≤ 45 μm)	23.5	11.7	5.9	0
Micro alumina (d ≤ 5 μm)	3	3	3	3
CAC	3	3	3	3
Microsilica	0.5	0.5	0.5	0.5
Water (addition)	5.2	5.2	5.8	5.8
Water reducer	0.02	0.02	0.02	0.02

Table 4. Chemical composition of slag (wt%).

Al_2O_3	CaO	MgO	SiO_2	Fe_2O_3	MnO	TiO_2
3.44	44.75	9.27	10.51	29.08	2.40	0.61

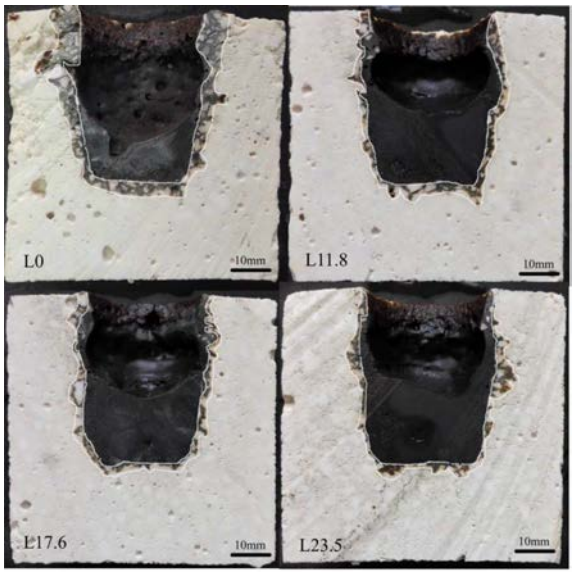

Fig. 2. Corrosion sections of the castables after the corrosion test, at 1600 ºC for 3 hrs in air.

Table 2. The lattice strains, lattice parameters and crystallite sizes of spinels in LBC and DBC and the phase compositions and particle sizes of LBC and DBC powders.

	Crystallite size (D, nm)	lattice parameter (a, nm)	Lattice strain (Δd/d, %)	Median particle size (d50, μm)	Phase composition (wt%)	
					Corundum	Spinel
Spinel in LBC	66.33	8.0429	0.194	–	–	–
Spinel in DBC	190.62	8.0653	0.070	–	–	–
LBC	–		–	2.13	68	32
DBC	–		–	20.18	64	36

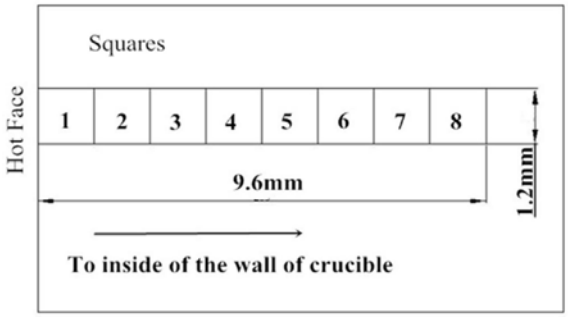

Fig. 3. Schematic diagram of 8 squares' distribution.

and penetration indexes were calculated by the image processing software, which was described by Yan [12]. In order to figure out the depth of slag penetration, CaO and Fe_2O_3 contents in the 8 squares from hot face to inside of the wall of crucibles were measured by SEM and energy dispersive X-ray spectroscope (EDS). The schematic diagram of 8 squares is shown in Fig. 3.

Characterization

The particle size distributions were measured by a laser particle size analyzer (Matersizer 2000). The phase composition and the lattice characteristics of spinel were measured by X-ray diffraction (X'Pert PRO MPD, Philips, Eindhoven, Netherlands) with a scanning speed of 2 º per minute. The relative contents of corundum and spinel were calculated by the semi-quantitative analysis in HighScore works on basis of the RIR (=Refrence Intensity Ratio) values. Lattice strain and crystallite size of spinel were calculated based on the Scherrer's Law using the X' Pert High Score software (version 3.0). The lattice parameter was calculated based on the formula $a^2\sin^2\theta = \theta^2(h^2 + k^2 + l^2)$. The apparent porosities (APs) and bulk densities (BDs) of castables were obtained by the Archimedes' principle with water as the medium. Pore size distribution (PSD) of matrices were obtained by a microscopy measurement method through an optical microscope (Axioskop40, Carl Zeiss, Germany). The microstructures and the compositions of the LBC and DBC grains and the liquid phases which are the penetrated slag in 8 squares of the samples corroded were investigated by a field emission scanning electron microscope (FE-SEM, Nova 400 NanoSEM, FEI Company, USA) equipped with energy dispersive X-ray spectroscope (EDS, INCA IE 350 Penta FET X-3, Oxford, UK). Simultaneously, the viscosities of the liquid phases at 1600 ºC were calculated by FactSage 6.2 thermal-chemical software. In this calculation, the databases of Fact 53 and FToxid were used.

Results and Discussion

Fig. 4 shows the corrosion and penetration indexes of the castables after slag corrosion test. It was found that with the increase of LBC content from 0 to 23.5 wt%,

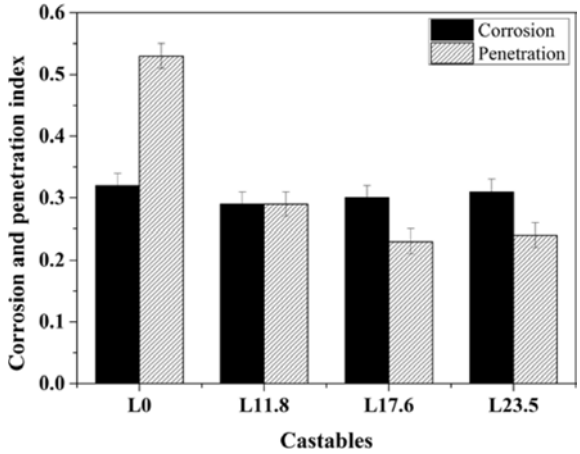

Fig. 4. Corrosion and penetration indexes of castables corroded at 1600 ºC for 3 hrs.

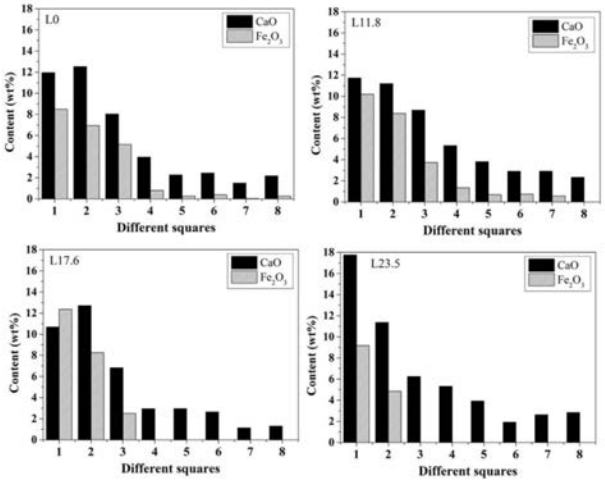

Fig. 5. CaO and Fe_2O_3 contents in different squares of the castables after slag corrosion test.

Table 5. Apparent porosities and bulk densities of castables.

	Apparent porosity (%)	Bulk density (g/cm^3)
L0	15.3(± 1)	3.15(± 0.02)
L11.8	15.8(± 1)	3.13(± 0.02)
L17.6	15.7(± 1)	3.13(± 0.02)
L23.5	15.7(± 1)	3.11(± 0.02)

the penetration index decreased and the penetration indexes of castables L17.6 and L23.5 were similar; the corrosion index decreased little with the increase of LBC content from 0 to 11.8 wt% but increased slowly when the LBC content increased from 11.8 wt% to 23.5 wt%. It means that LBC can efficiently enhance the penetration resistance but has little effect on corrosion resistance. Considering the corrosion and penetration resistances, the optimized LBC content is 17.6 wt%.

The CaO and Fe_2O_3 contents in different squares of the castables after slag test are presented in Fig. 5, which can express the depth of slag penetration. For

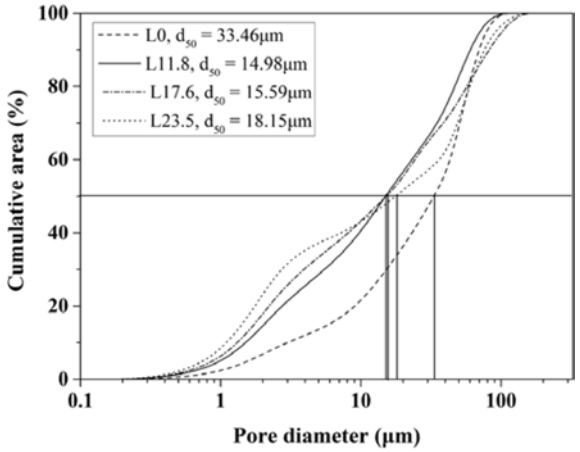

Fig. 6. Pore size distributions of matrices of castables.

castables L0, Fe_2O_3 was detected in all the 8 squares; it means that the penetration of slag has reached to square 8. For L11.8, Fe_2O_3 was not detected in square 8. Fe_2O_3 was only detected in squares 1, 2, 3 of sample L17.6. For sample L23.5, there was no Fe_2O_3 found in square 3. It indicates that the depths of slag penetration decrease with the increase of LBC contents of the castable samples. At the same time, the contents of Fe_2O_3 in squares 1 of sample L23.5 is higher than that of the other samples; it means that the LBC can absorb more Fe and Mn ions than DBC. Compared with the penetration of Fe_2O_3 in slag, CaO penetrates more deeply. In conclusion, the penetration resistances of castables with LBC are higher than that without it, which is in accordance with the results shown in Fig. 4.

LBC gives three possible impacts on the slag resistance of corundum-spinel castables: (1) The LBC content changes the APs of castables and PSDs of matrices [12, 14, 15] through changing the packing behavior of powders; (2) The spinel in LBC with higher lattice strain and smaller crystallite size could absorb more Mn and Fe ions, and thus increasing the viscosities of the penetrated slag [7, 12, 16]; (3) The LBC content affects the average particle sizes of the matrices, which affects the dissolution rate of the particles in matrices into slag [8].

Table 6 gives the APs and BDs of castables. It is found that the APs of the four castables are almost the same. It means that the effect of AP can be ignored.

Fig. 6 and Fig. 7 show the pore diameter distributions of the matrices and typical micrographs of matrices in original layers of castables, respectively. Castable L0 has the largest median pore diameter (MPD, d50) which

Table 6. EDS results of grains of DBC and LBC in the first 5 squares of castables (wt%).

Squares	Samples	Spinels	Compositions					$MnO + Fe_2O_3$
			Al_2O_3	CaO	MgO	MnO	Fe_2O_3	
1	L11.8	DBC	63.16	0.00	23.54	1.77	11.52	13.29
		LBC	43.64	6.28	18.60	2.63	26.63	29.26
	L17.6	DBC	62.14	–	23.92	2.18	11.76	13.94
		LBC	50.43	1.63	22.77	2.36	22.81	25.17
	L23.5	LBC	58.06	–	21.58	3.15	17.22	20.37
2	L11.8	DBC	61.98	0.46	24.91	1.86	10.79	12.65
		LBC	56.82	0.46	24.60	2.22	15.35	17.57
	L17.6	DBC	59.72	1.00	20.80	2.75	16.73	19.48
		LBC	53.11	–	18.56	3.20	24.51	27.71
	L23.5	LBC	57.80	0.62	19.36	3.85	18.99	22.84
3	L11.8	DBC	62.72	2.06	22.43	1.66	11.13	12.79
		LBC	59.40	1.18	20.84	–	14.62	14.62
	L17.6	DBC	59.22	3.18	19.62	2.59	13.36	15.95
		LBC	60.11	1.88	18.96	2.47	15.68	18.15
	L23.5	LBC	80.54	3.30	11.02	–	0.00	–
4	L11.8	DBC	69.09	–	21.30	1.96	7.64	9.60
		LBC	68.25	–	20.88	2.08	8.78	10.86
	L17.6	DBC	66.14	0.59	20.08	2.10	11.08	13.18
		LBC	63.72	–	21.54	2.33	12.40	14.73
	L23.5	LBC	81.06	4.41	11.64	–	0.00	–
5	L11.8	DBC	72.70	0.85	24.97	–	1.48	1.48
		LBC	70.79	0.72	24.95	–	1.66	2.05
	L17.6	DBC	78.10	1.76	20.15	–	–	–
		LBC	69.36	3.58	21.35	–	–	–
	L23.5	LBC	71.58	1.35	24.30	–	–	–

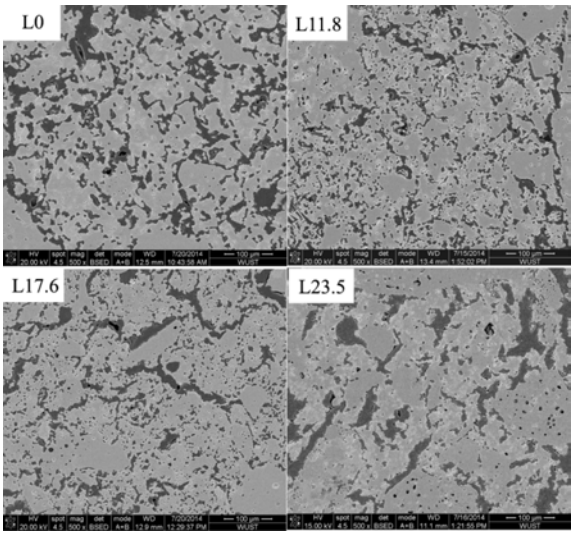

Fig. 7. Typical micrographs of matrices in original layers of castables.

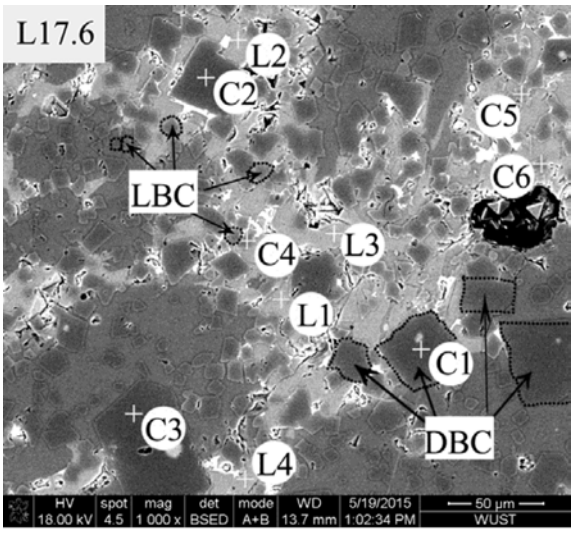

Fig. 8. A typical SEM micrograph of matrix in square 1 of sample L17.6 after corrosion test. L: liquid, C: alumina-spinel composite.

may result from the larger particle size of DBC. The packing with larger size particles forms larger size pores among the particles [17]. This maybe one of the possible reasons why castable L0 has the highest penetration index. However, castable L11.8 has the lowest MPD, but higher penetration index. At the same time, the MPDs of castables L17.6 and L23.5 are higher than that of L11.8, but the penetration indexes of castables L17.6 and L23.5 are lower than that of castable L11.8 (Fig. 4). It means that the pore diameter is one but not the most important factor affecting the penetration resistance in this study.

Fig. 8 shows a typical SEM micrograph of matrix in square 1 of castable L17.6 after corrosion test. The light grey grains are LBC (refer to C1 ~ C3) with small size (d50 = 2.13 μm). The dark grey grains are DBC (refer to C4 ~ C6) with bigger size (d50 = 20.18 μm). The bright phases (refer to L1 to L4) are liquid phases formed by interaction between slag and refractories.

In order to compare the differences of ($MnO + Fe_2O_3$) contents between the BDC and LBC grains in the castables, the EDS results which are the average value of 3 grains are given in Table 6. It is found that the ($MnO + Fe_2O_3$) contents of LBC grains are higher than those of DBC grains in all the squares, because the spinels in LBC have higher lattice strain and smaller crystallite size. It is another possible reason that LBC powder has smaller particle size [18]. At the same time, the differences of ($MnO + Fe_2O_3$) contents between LBC and DBC grains decrease from square 1 to square 5, because ($MnO + Fe_2O_3$) content of penetrated slag reduces with increase of penetrated deepness of slag.

Table 7. Compositions and viscosities of liquid phases at 1600°C in the first 5 squares of castables (wt%).

Squares	Samples	Compositions							Viscosities (Pa·S)
		SiO_2	Al_2O_3	CaO	MgO	Na_2O	MnO	Fe_2O_3	
1	L11.8	20.04	36.29	38.04	0.62	–	–	5.00	0.151
	L17.6	22.17	33.75	37.95	–	–	–	6.13	0.153
	L23.5	21.65	35.34	34.08	1.92	–	–	7.00	0.156
2	L11.8	21.84	35.14	38.36	–	0.19	–	4.47	0.157
	L17.6	10.90	58.46	18.72	2.53	-	0.93	8.46	0.175
	L23.5	17.25	45.24	29.13	4.63	-	–	3.74	0.184
3	L11.8	21.25	38.45	34.77	–	-	–	5.52	0.164
	L17.6	9.34	62.88	10.17	10.97	-	–	6.64	0.241
	L23.5	9.17	65.85	8.58	13.92	2.48	–	-	0.249
4	L11.8	27.43	28.89	39.85	–	1.61	–	2.22	0.183
	L17.6	8.23	73.78	6.80	5.41	–	–	5.77	0.245
	L23.5	9.53	69.87	9.72	9.66	1.22	–	-	0.250
5	L11.8	7.52	69.92	6.55	13.06	1.67	–	1.26	0.249
	L17.6	7.43	68.27	4.48	18.28	–	–	1.54	0.266
	L23.5	10.38	67.01	6.92	13.88	1.81	–	–	0.265

The compositions which are the average value of 4 grains obtained by EDS and the viscosities obtained by FactSage 6.2 in the first 5 squares of the castables are given in Table 7. In the square 1, the differences of viscosities of the liquids among castables L11.8, L17.6 and L23.5 are a little, because a large amount of the original slag in this square results in a little change of the compositions of liquids in the castables. However, in the squares 2, 3, 4 and 5, the viscosities of the penetrated slags in the castables increase with the increase of LBC content. The difference in the viscosities of castables L11.8 and L17.6 is bigger, while the difference between L17.6 and L23.5 is smaller. This difference may result from the different reaction degree between slag and refractory which can influence the compositions and viscosities of the penetrated slags. As we can see from Table 7, the difference in the compositions of the penetrated slags among square 3, 4 and 5 of castable L17.6 and L23.5 is relatively smaller. The smaller the difference in compositions of the penetrated slag among different squares of the same castable, the closer the reaction near to equilibrium. It means the reaction between slag and castable L17.6/L23.5 is near to equilibrium in the square 3, whereas the reaction degree in the square 5 of castable L11.8 is difficult to estimate. Obviously, the effect of the viscosity of the penetrated slag on the penetration resistance is in accordance with the results shown in Fig. 4. It indicates that the viscosity of the penetrated slag has a more significant impact on the penetration resistance than the other factors in the present work.

Based on the results mentioned above, it can be indicated that the effect of LBC on the penetration resistance take place in the squares 2, 3 and 4. The spinel grains with higher lattice strains, smaller crystallite and particle sizes in LBC absorb more Mn and Fe ions from the penetrated slag and increase the viscosity of slag, resulting in the increase of penetration resistance.

Corrosion resistance depends on the dissolution rate of castable into slag which relates to the particle size, crystallite size, the phase composition and slag penetration. Among these aspects, phase composition can be ignored because the phase compositions of LBC and DBC are similar (Table 2). Comparing with the DBC, the smaller particle and crystallite sizes of LBC (Table 2) would result in its higher dissolution rate into slag [18]. But the lower slag penetration reduces the contact area between slag and refractory (Fig. 3) and decreases the dissolution rate of refractory into slag. Therefore, a compromise reached among these aspects may be the reason why the corrosion resistances of castables changed little.

Conclusions

The effect of light-burned alumina-spinel composite (LBC) with 90 wt% of Al_2O_3 content on the penetration and corrosion resistances of corundum-spinel castables was studied. The major results are summarized as follows:

1. The LBC with 90 wt% of Al_2O_3 content can improve penetration resistance but has little effect on corrosion resistance of corundum-spinel castable. The optimized balance between penetration resistance and corrosion resistance of castable is the content of 17.6 wt% of LBC.

2. The spinel in LBC absorb more Fe and Mn ions from slag than that in dead-burned alumina-spinel composite (DBC) because of its smaller crystallite size and larger lattice strain, resulting in the increase of viscosity of penetrated slag and penetration resistance. With the penetration depth increasing, the difference between LBC and DBC becomes smaller.

Acknowledgments

The authors would like to thank the National Natural Science Foundation of China (Grant No. 51572203) and the Key Program of Natural Science Foundation of Hubei Province of China (Grant No. 2015CFA122) for financially supporting this work.

References

1. Y. Zou, H. Gu, A. Huang, M. Zhang, C. Ji, Ceram. Int. 40[5] (2014) 7023-7028.
2. L. Fu, H. Gu, A. Huang, M. Zhang, X. Hong, L. Jin, Ceram. Int. 41[1] Part B (2015) 1263-1270.
3. L. Fu, H. Gu, A. Huang, C. Bai, Ceram. Int. 41[4] (2015) 5857-5862.
4. A.G.T. Martinez, A.P. Luz, M.A.L. Braulio, V.C. Pandolfelli, Ceram. Int. 41[3] Part B (2015) 4714-4725.
5. T.M. Souza, A.P. Luz, V.C. Pandolfelli, Ceram. Int. 40[9] Part B (2014) 14947-14956.
6. I. Ganesh, S. Bhattacharjee, B. Saha, R. Johnson, K. Rajeshwari, R. Sengupta, M.R. Rao, Y. Mahajan, Ceram. Int. 28 [3] (2002) 245-253.
7. H. Sarpoolaky, S. Zhang, W. Lee, J. Eur. Ceram. Soc. 23[2] (2003) 293-300.
8. M. Braulio, L. Bittencourt, V. C. Pandolfelli, J. Eur. Ceram. Soc. 28[15] (2008) 2845-2852.
9. E.Y. Sako, M.A.L. Braulio, V.C. Pandolfelli, Ceram. Int. 38[3] (2012) 2177-2185.
10. M. Fuhrer, A. Hey, W. Lee, J. Eur. Ceram. Soc. 18[7] (1998) 813-820.
11. X.M. Fang, N. Li, W. Yan, Naihuo Cailiao. 45 (2011) 14-17.
12. W. Yan, J. Chen, N. Li, W. Qiu, J. Ouyang, X. He, J. Ceram. Process. Res. 15 [6] (2014) 441-446.
13. M.A. Sainz, A.D. Mazzoni, E.F. Aglietti, A. Caballero, Mater. Chem. Phys. 86[2-3] (2004) 399-408.
14. M.A.L. Braulio, A.G.T. Martinez, A.P. Luz, C. Liebske, V.C. Pandolfelli, Ceram. Int. 37[6] (2011) 1935-1945.
15. E.Y. Sako, M.A. L. Braulio, E. Zinngrebe, S.R. van der Laan, V.C. Pandolfelli, Ceram. Int. 38[3] (2012) 2243-2251
16. Y.-C Ko, Ceram. Int. 28[7] (2002) 805-810
17. R.M. German, "Sintering Theory and Practice", The Ronald Press (1995) 181-183.
18. J. Mori, N. Watanabe, M. Yoshimura, Y. Oguchi, T. Kawakami, Am. Ceram. Soc. Bull. 69[7] (1990)1172-1176.